J|A|C|S
ARTICLES
Published on Web 10/09/2004

Five-Coordinate $Fe^{III}NO$ and $Fe^{II}CO$ Porphyrinates: Where Are the Electrons and Why Does It Matter?

Douglas P. Linder,[†] Kenton R. Rodgers,*[,†] Jennifer Banister,[†] Graeme R. A. Wyllie,[‡] Mary K. Ellison,[‡] and W. Robert Scheidt[‡]

Contribution from the Department of Chemistry and Molecular Biology, North Dakota State University, Fargo, North Dakota 58105, and Department of Chemistry and Biochemistry, University of Notre Dame, Notre Dame, Indiana 46556

Received May 24, 2004; E-mail: Kent.Rodgers@ndsu.nodak.edu

Abstract: Recent years have seen dramatic growth in our understanding of the biological roles of nitric oxide (NO). Yet, the fundamental underpinnings of its reactivities with transition metal centers in proteins and enzymes, the stabilities of their structures, and the relationships between structure and reactivity remains, to a significant extent, elusive. This is especially true for the so-called ferric heme nitrosyls ($\{FeNO\}^6$ in the Enemark−Feltham scheme). The Fe−CO and C−O bond strengths in the isoelectronic ferrous carbonyl complexes are widely recognized to be inversely correlated and sensitive to structural, environmental, and electronic factors. On the other hand, the Fe−NO and N−O bonds in $\{FeNO\}^6$ heme complexes exhibit seemingly inconsistent behavior in response to varying structure and environment. This report contains resonance Raman and density functional theory results that suggest a new model for FeNO bonding in five-coordinate $\{FeNO\}^6$ complexes. On the basis of resonance Raman and FTIR data, a direct correlation between the ν_{Fe-NO} and ν_{N-O} frequencies of $[Fe(OEP)NO](ClO_4)$ and $[Fe(OEP)NO](ClO_4)\cdot CHCl_3$ (two crystal forms of the same complex) has been established. Density functional theory calculations show that the relationship between Fe−NO and N−O bond strengths is responsive to FeNO electron density in *three* molecular orbitals. The highest energy orbital of the three is σ-antibonding with respect to the entire FeNO unit. The other two comprise a lower-energy, degenerate, or nearly degenerate pair that is π-bonding with respect to Fe−NO and π-antibonding with respect to N−O. The relative sensitivities of the electron density distributions in these orbitals are shown to be consistent with all published indicators of Fe−N−O bond strengths and angles, including the examples reported here.

Introduction

Interactions of the diatomic ligands CO, NO, and O_2 with heme proteins and enzymes form the basis of many biological processes. The functions of these hemes are almost always distinguished by their protein environments. The rich diversity of heme reactivity derives from the broad spectrum of bonded and nonbonded interactions between the heme, its axial ligands (i.e., FeXO moieties, where X = C, N, O), and the heme pockets of proteins.[1] Therefore, an understanding of heme FeXO bonding is pivotal to understanding the interplay between structure and function of many heme proteins. Of the π-acid ligands, NO and CO, NO appears to play more crucial roles in the biology of mammals.[2] The bonding between NO and iron in heme proteins is an important aspect of neurotransmission, vasodilation, blood clotting, and immunoresponse.[3−5] Additionally, the vasodilating effect of NO in mammals is exploited by the blood-sucking insect *Rhodnius prolixus*, which delivers NO to the tissues of its victim as a means of maintaining blood flow near the site of its bite. Delivery is accomplished by the NO adduct of ferric heme proteins called nitrophorins (NPs), which are components of the insect's saliva.[6,7] The chemistry of tetrapyrrolic $\{FeNO\}^6$ complexes is also thought to play critical roles in denitrification.[8] Much has been learned of the FeXO interactions from infrared (IR) and resonance Raman (rR) vibrational studies.[9] The ligand−protein interactions can be assessed on the basis of their Fe−XO and X−O vibrational frequencies and their sensitivities to the composition and environment (nonbonded interactions) of the complex.

A large body of data from many IR and Raman studies has revealed an *inverse* or indirect correlation between the ν_{Fe-XO} and ν_{X-O} frequencies for Fe(II) systems.[10−16] In other words,

[†] North Dakota State University.
[‡] University of Notre Dame.

(1) Jain, R.; Chan, M. K. *J. Biol. Inorg. Chem.* **2003**, *8*, 1−11.
(2) Culotta, E.; Koshland, D. E., Jr. *Science* **1992**, *258*, 1862−1865.
(3) Cooper, C. E. *Biochim. Biophys. Acta* **1999**, *1411*, 290−309.
(4) *Methods in Nitric Oxide Research*; Feelisch, M., Stamler, J. S. Eds.; Wiley: Chichester, 1996.
(5) Moncada, S.; Palmer, R. M.; Higgs, E. A. *Pharmacol. Rev.* **1991**, *43*, 109−142.
(6) (a) Ding, X. D.; Weichsel, A.; Anderson, J. F.; Shokhireva, T., Kh.; Balfour, C.; Pierik, A. J.; Averill, B. A.; Montfort, W. R.; Walker, F. A. *J. Am. Chem. Soc.* **1999**, *121*, 128−138. (b) Ribeiro, J. M. C.; Hazzard, J. M. H.; Nussenzveig, R. H.; Champagne, D. E.; Walker, F. A. *Science* **1993**, *260*, 539−541.
(7) Roberts, S. A.; Weichsel, A.; Qiu, Y.; Shelnutt, J. A.; Walker, F. A.; Montfort, W. R. *Biochemistry* **2001**, *40*, 11327−11337.
(8) Averill, B. A. *Chem. Rev.* **1996**, *96*, 2951−2964.
(9) Rousseau, D. L.; Ondrias, M. R. In *Optical Techniques in Biological Research*; Rousseau, D. L., Ed.; Academic Press: Orlando, FL,1984; pp 65−132.

10.1021/ja046942b CCC: $27.50

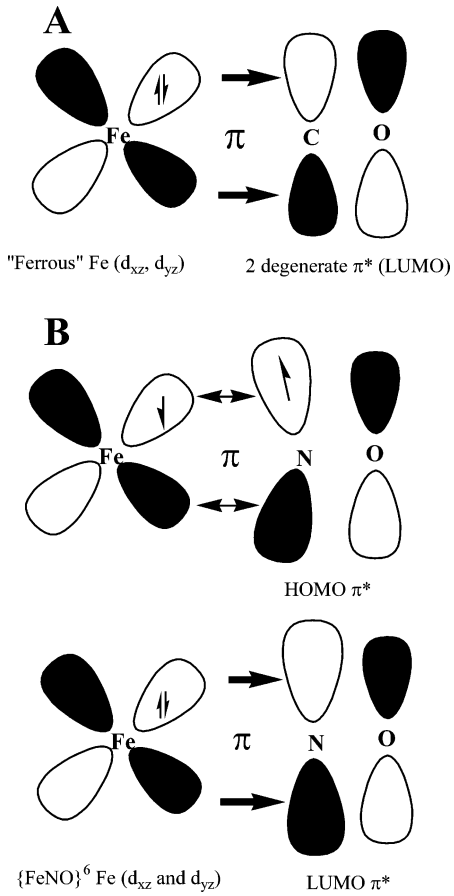

Figure 1. Simplified valence orbital scheme illustrating the π-interactions between (A) Fe(II) and CO and (B) Fe(III) and NO.

factors that cause one frequency to increase cause the other to decrease, and vice versa. This relationship has long been recognized in Fe(II)CO porphyrinates and has been attributed to variations in π-back-donation (back-bonding) between the occupied d_π orbitals of Fe(II) and the empty π^* orbitals of CO.[17,18] A widely invoked bonding model of the π-orbital interactions is shown in Figure 1 for Fe(II)CO systems. In this model, π-back-bonding increases the Fe−C bond order while decreasing that of C−O. The extent of back-bonding is responsive to several factors, including nonbonded interactions with heme pocket residues that can polarize the bound CO ligand (distal or environmental effects), solvent polarity, and the electron-donating or electron-withdrawing nature of porphyrin

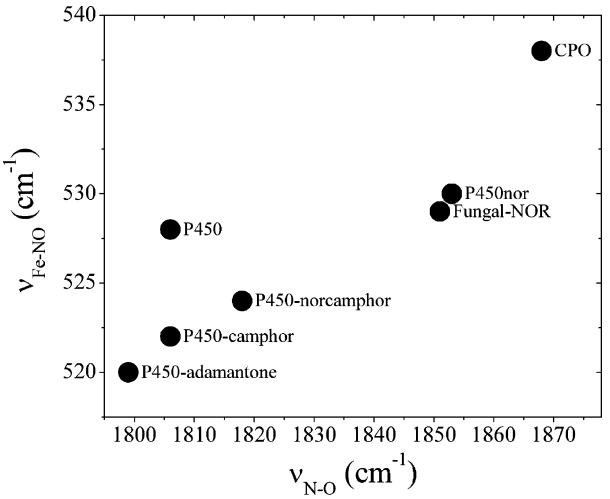

Figure 2. Experimental vibrational stretching frequency correlation ν_{Fe-NO} vs ν_{N-O} based on published data. All points represent six-coordinate {FeNO}^{6} complexes with an axial thiolate ligand trans to NO; chloroperoxidase (CPO),[21c,22] cytochrome P450-nor,[22] fungal NOR,[21a] P450, P450-norcamphor, P450-camphor, and P450-adamantone.[21b,22]

substituents (cis effects).[18] The valence-orbital interactions are distinct for the isoelectronic Fe(III)NO system, as illustrated at the bottom of Figure 1. For Fe(III)NO there is still π-back-bonding between a single two-electron Fe d_π orbital and the empty NO π^* orbital. The other d_π orbital is half filled and can form a more covalent bond with the lone π^* electron in the HOMO of NO. In this description, these two electrons are delocalized between Fe and NO. This interaction increases the Fe−NO bond order with a concomitant increase in the N−O bond order as a result of the diminished electron density in the NO π^* orbital.[19] However, which of these effects would dominate the relative sensitivities of the Fe−NO and N−O bond strengths in response to endogenous or exogenous factors is not at all clear from this model.

Additionally, for the most studied case of Fe(II)CO, there are distinct inverse correlation lines for different trans axial (proximal) ligand types. Three classes of Fe(II)CO complexes have been identified having histidine (neutral), thiolate or imidazolate (anionic), or very weak trans axial ligand fields. The biasing of the correlation lines is thought to arise from a competition between the trans axial ligand and CO for the Fe d_z^2 orbital, and since σ donor strength generally correlates with proximal ligand charge, it plays a defining role in this trans effect.[18]

Though it is tempting to extrapolate the valence orbital model of the Fe−C−O bonding to the isoelectronic Fe(III)NO (hereinafter indicated by the Enemark and Feltham notation,[20] {FeNO}^{6}) systems, this report presents experimental and computational evidence that suggests a more elegant, albeit complex, relationship between the Fe−NO and N−O bond strengths. Figure 2 shows a plot of ν_{Fe-NO} versus ν_{N-O} for

(10) Coyle, C. M.; Vogel, K. M.; Rush, T. S., III; Kozlowski, P. M.; Williams, R.; Spiro, T. G.; Dou, Y.; Ikeda-Saito, M.; Olson, J. S.; Zgierski, M. Z. *Biochemistry* **2003**, *42*, 4896−4903.
(11) Andrew, C. R.; Green, E. L.; Lawson, D. M.; Eady, R. R. *Biochemistry* **2001**, *40*, 4115−4122.
(12) (a) Vogel, K. M.; Kozlowski, P. M.; Zgierski, M. Z.; Spiro, T. G. *J. Am. Chem. Soc.* **1999**, *121*, 9915−9921. (b) Vogel, K. M.; Kozlowski, P. M.; Zgierski, M. Z.; Spiro, T. G. *Inorg. Chim. Acta* **2000**, *297*, 11−17.
(13) (a) Ray, G. B.; Li, X.-Y.; Ibers, J. A.; Sessler, J. L.; Spiro, T. G. *J. Am. Chem. Soc.* **1994**, *116*, 162−176. (b) Li, X.-Y.; Spiro, T. G. *J. Am. Chem. Soc.* **1988**, *110*, 6024−6033. (c) Spiro, T. G.; Smulevich, G.; Su, C. *Biochemistry* **1990**, *29*, 4497−4508.
(14) Lukat-Rodgers, G. S.; Wengenack, N. L.; Rusnak, F.; Rodgers, K. R. *Biochemistry* **2001**, *40*, 7149−7157.
(15) (a) Park, E. S.; Thomas, M. R.; Boxer, S. G. *J. Am. Chem. Soc.* **2000**, *122*, 12297−12303. (b) Thomas, M. R.; Brown, D.; Frazen, S.; Boxer, S. G. *Biochemistry* **2001**, *40*, 15047−15056.
(16) Phillips, G. N.; Teodoro, M. L.; Li, T.; Smith, B.; Olson, J. S. *J. Phys. Chem. B* **1999**, *103*, 8817−8829.
(17) Buchler, J. W.; Kokisch, W.; Smith P. D. *Struct. Bonding* **1978**, *34*, 79−134.
(18) Spiro, T. G.; Zgierski, M. Z.; Kozlowski, P. M. *Coord. Chem. Rev.* **2001**, *219*−*221*, 923−936.
(19) Wang, J.; Caughey, W. S.; Rousseau, D. L. In *Methods in Nitric Oxide Research*; Feelisch, M., Stamler, J. S., Eds.; Wiley: Chichester, 1996; pp 427−454.
(20) The {FeNO}^{n} nomenclature of Enemark and Feltham is used here to avoid the ambiguities surrounding assignment of an Fe oxidation state for NO-coordinated complexes is not unambiguous. In {FeNO}^{n} the "*n*" represents the number of iron atom d-electrons plus the lone π^* electron from the nitrosyl ligand. Using this nomenclature the "ferric" or Fe(III) nitrosyl systems are classified as {FeNO},^{6} whereas the "ferrous" or Fe(II) nitrosyls are classified as {FeNO}^{7} systems. Enemark, J. H.; Feltham, R. D. *Coord. Chem. Rev.* **1974**, *13*, 339−406.

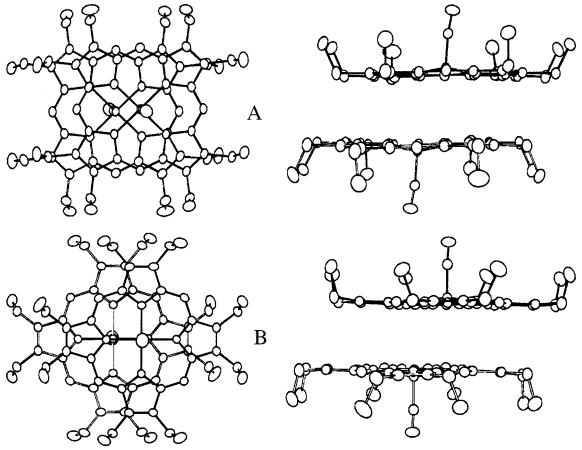

Figure 3. Structures of (A) [Fe(OEP)(NO)]ClO_4, **1**, and (B) [Fe(OEP)(NO)]ClO_4·$CHCl_3$, **1·CHCl$_3$**.

characterized {FeNO}^{6} systems.[21,22] Even from this limited number of points, which correspond to {FeNO}^{6} hemes having thiolate ligands trans to NO, it is evident that their ν_{Fe-NO} and ν_{N-O} frequencies are *directly* correlated. This correlation is distinct from that of the isoelectronic Fe(II)CO thiolate systems[22] and cannot be clearly explained by the π-back-bonding model. The goal of this study is to elucidate the basis of this distinction. Herein, we report the investigation of two crystal forms of the five-coordinate [Fe(OEP)(NO)]ClO_4 complex (Figure 3) by IR and rR spectroscopy. These results show a *direct* correlation between ν_{Fe-NO} and ν_{N-O} that is consistent with the behavior illustrated in Figure 2. This suggests that the correlation is an intrinsic property of the {FeNO}^{6} porphyrin systems, as opposed to a distal effect of different protein environments. Additionally, theoretical data from quantum chemical calculations on model five-coordinate {FeNO}^{6} porphyrin systems are presented. These calculations not only reproduce the *direct* ν_{Fe-NO} versus ν_{N-O} correlation, but the molecular orbitals reveal the nature of its origin, which can only be explained by invoking highly delocalized orbitals. To our knowledge, this is the first systematic examination of the *direct* ν_{Fe-NO} versus ν_{N-O} vibrational frequency correlation in five-coordinate {FeNO}^{6} porphyrin systems from a theoretical and/or experimental perspective.

The theoretical techniques used in this study are based on the density functional theory (DFT) of Hohenberg, Kohn, and Sham.[23,24] The accurate computation of geometries, vibrational frequencies, and energies of transition-metal-containing systems is known to require extensive electron correlation techniques. The DFT methods, incorporating nonlocal exchange and correlation functionals, have demonstrated the ability to account for much of this electron correlation.[25] Moreover, DFT methods show promise for the study of large systems of biochemical interest, as electron correlation effects can be included at a fraction of the computational cost of traditional ab initio methods. These methods have recently been applied to a number of iron nitrosyl porphyrinates.[26]

Methods

Sample Preparation. The five-coordinate {FeNO}^{6} complexes, [Fe(OEP)(NO)]ClO_4 (**1**) and [Fe(OEP)(NO)]ClO_4·$CHCl_3$ (**1·CHCl$_3$**), were prepared according to the literature methods.[27] The five-coordinate ^{15}NO complex, [Fe(OEP)(^{15}NO)]ClO_4 (**^{15}1**), was prepared by placing a rigorously degassed CH_2Cl_2 solution of [Fe(OEP)$OClO_3$] under 1 atm of ^{15}NO. Upon mixing, an immediate color change from brown to reddish-purple was observed. Microcrystalline [Fe(OEP)(^{15}NO)]ClO_4 was then precipitated by addition of hexane. The solvents were removed by a stream of N_2 gas.

Raman Spectroscopy. rR spectra were collected on a spectrometer equipped with a liquid N_2 cryostat that has been previously described.[28] The rR spectra were acquired using 406.7-nm excitation from a krypton ion laser. Laser powers were controlled between 0.5 and 40 mW at the sample. The sampling method consisted of a thin layer of the microcrystalline sample spun at ~20 Hz in a 5-mm NMR tube at −40 °C. The acquisition time for each sample was 1 h. The spectrometer was calibrated using Raman bands of toluene and methylene bromide as frequency standards.

Electronic Structure Calculations. The DFT calculations were performed using the hybrid exchange-correlation functional B3LYP, as implemented in Gaussian 98.[29] This functional is Becke's three-parameter exchange functional, in conjunction with the nonlocal correlation functional of Lee, Yang, and Parr.[30] All results were obtained from the all-electron restricted Kohn−Sham calculations for the systems of singlet spin multiplicity. For these two complexes, experimental Mössbauer results indicate a diamagnetic ground state.[27]

The 6-31G(d) basis set was used for all atoms except Fe, for which the all-electron basis set of Wachters and Hay (6-311+G) with the scaling factors of Ragavachari and Trucks was used.[31] In all calculations, an ultrafine integration grid was used to ensure numerical accuracy.

The DFT calculations were performed under C_s symmetry constraints unless otherwise stated. The plane of symmetry includes the Fe−N−O unit and bisects adjacent Fe−N(pyrrole) (Fe−N_p) bonds, a geometry close to that in the reported X-ray structure of **1**.[27]

The B3LYP method has been used and parameterized extensively on smaller systems where accurate vibrational frequencies are known.[32] For this method, several linear scaling factors have been used for the computation of harmonic vibrational frequencies with the different scaling factors arising out of the different atomic and molecular data

(21) (a) Shimizu, H.; Obayashi, E.; Gomi, Y.; Arakawa, H.; Park, S.-Y.; Nakamura, H.; Adachi, S.; Shoun, H.; Shiro, Y. *J. Biol. Chem.* **2000**, *275*, 4816−4826. (b) Hu, S.; Kincaid, J. R. *J. Am. Chem. Soc.* **1991**, *113*, 2843−2850. (c) Hu, S.; Kincaid, J. R. *J. Biol. Chem.* **1993**, *268*, 6189−6193.

(22) Obayashi, E.; Tsukamato, K.; Adachi, S.; Takahashi, S.; Nomura, M.; Iizuka, T.; Shoun, H.; Shiro, Y. *J. Am. Chem. Soc.* **1997**, *119*, 7807−7816.

(23) (a) Hohenberg, P.; Kohn, W. *Phys. Rev. B* **1964**, *136*, 864−871. (b) Kohn, W.; Sham, L. *Phys. Rev. A* **1965**, *140*, 1133−1138.

(24) Parr, R. G.; Yang, W. *Density-Functional Theory of Atoms and Molecules*; Oxford University Press: New York, 1989.

(25) (a) Ziegler, T. *Chem. Rev.* **1991**, *91*, 651−657. (b) Siegbahn, P. E. M.; Blomberg, M. R. A. *Annu. Rev. Phys. Chem.* **1999**, *50*, 221−249.

(26) (a) Leu, B. M.; Zgierski, M. Z.; Wyllie, G. R. A.; Scheidt, W. R.; Sturhahn, W.; Alp, E. E.; Durbin, S. M.; Sage, J. T. *J. Am. Chem. Soc.* **2004**, *126*, 4211−4227. (b) Zhang, Y.; Gossman, W.; Oldfield, E. *J. Am. Chem. Soc.* **2003**, *125*, 16387−16396.

(27) Ellison, M. K.; Schulz, C. E.; Scheidt, W. R. *Inorg. Chem.* **2000**, *39*, 5102−5110.

(28) Rodgers, K. R.; Lukat-Rodgers, G. S.; Tang, L. *J. Biol. Inorg. Chem.* **2000**, *5*, 642−654.

(29) Frisch, M. J.; Trucks, G. W.; Schlegel, H. B.; Scuseria, G. E.; Robb, M. A.; Cheeseman, J. R.; Zakrzewski, V. G.; Montgomery, J. A., Jr.; Stratmann, R. E.; Burant, J. C.; Dapprich, S.; Millam, J. M.; Daniels, A. D.; Kudin, K. N.; Strain, M. C.; Farkas, O.; Tomasi, J.; Barone, V.; Cossi, M.; Cammi, R.; Mennucci, B.; Pomelli, C.; Adamo, C.; Clifford, S.; Ochterski, J.; Petersson, G. A.; Ayala, P. Y.; Cui, Q.; Morokuma, K.; Malick, D. K.; Rabuck, A. D.; Raghavachari, K.; Foresman, J. B.; Cioslowski, J.; Ortiz, J. V.; Stefanov, B. B.; Liu, G.; Liashenko, A.; Piskorz, P.; Komaromi, I.; Gomperts, R.; Martin, R. L.; Fox, D. J.; Keith, T.; Al-Laham, M. A.; Peng, C. Y.; Nanayakkara, A.; Gonzalez, C.; Challacombe, M.; Gill, P. M. W.; Johnson, B. G.; Chen, W.; Wong, M. W.; Andres, J. L.; Head-Gordon, M.; Replogle, E. S.; Pople, J. A. *Gaussian 98*, revision A.11.4; Gaussian, Inc.: Pittsburgh, PA, 2002.

(30) (a) Becke, A. D. *J. Chem. Phys.* **1993**, *98*, 5648−5652. (b) Lee, C. T.; Yang, W. T.; Parr, R. G. *Phys. Rev. B* **1988**, *37*, 785−789. (c) Stephens, P. J.; Devlin, F. J.; Chablowski, C. F.; Frisch, M. J. *J. Phys. Chem.* **1994**, *98*, 11623−11627.

(31) (a) Raghavachari, K.; Trucks, G. W. *J. Chem. Phys.* **1989**, *91*, 1062−1065. (b) Wachters, A. J. H. *J. Chem. Phys.* **1970**, *52*, 1033−1036. (c) Hay, P. J. *J. Chem. Phys.* **1977**, *66*, 4377−4384.

(32) Bauschlicher, C. W., Jr.; Partridge, H. *Chem. Phys. Lett.* **1995**, *240*, 533−540.

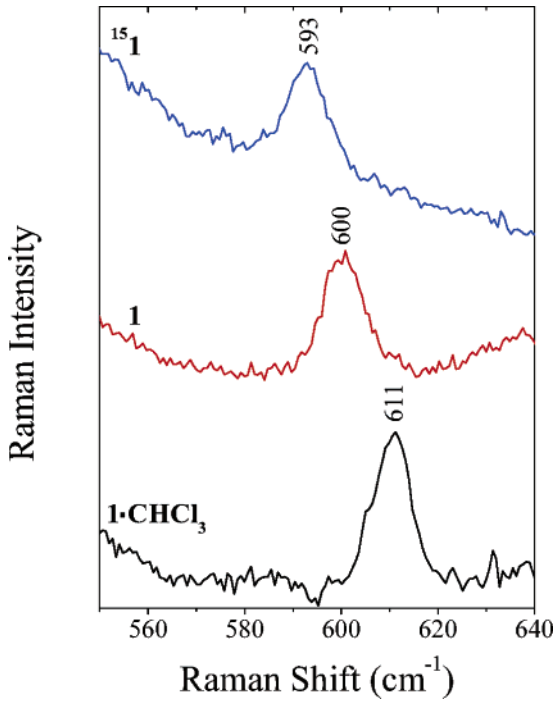

Figure 4. Resonance Raman spectra showing the ν_{Fe-NO} bands for the five-coordinate {FeNO}^{6} complexes [Fe(OEP)(NO)]ClO$_4$ (**1**), [Fe(OEP)-(^{15}NO)]ClO$_4$ (**^{15}1**), and [Fe(OEP)(NO)]ClO$_4$·CHCl$_3$ (**1·CHCl$_3$**). Excitation wavelength was 406.7 nm, $T = -40$ °C.

sets used.[33] In the present calculations, we used the linear scaling factor of 0.961 for the computation of harmonic vibrational frequencies, as reported for the B3LYP/6-31G(d) method.[33]

The following discussion involves significant comparison of five-coordinate [Fe(III)(Porph)NO]$^+$ complexes with their five-coordinate [Fe(II)(Porph)CO] analogues. This comparison is appropriate because these two systems are isoelectronic and their Fe-X−O geometries both tend to be linear or nearly linear. Additionally, the [Fe(II)(Porph)CO] systems have been extensively studied, and their inverse ν_{Fe-CO} versus ν_{C-O} correlation is very well-established. The DFT calculations performed on the [Fe(Porph)CO] systems reported here were carried out in the same manner as described for the [Fe(Porph)NO]$^+$ systems.

Results

Low-frequency Soret-excited rR spectra of **1** and **1·CHCl$_3$** are shown in Figure 4. The band at 600 cm^{-1} in the spectrum of **1** is assigned to the Fe−NO stretching vibration, ν_{Fe-NO}. The FTIR spectrum of **1** exhibits ν_{N-O} at 1838 cm^{-1}.[27] The assignments for **1** were verified with isotopic ^{15}NO substitution, for which $\nu_{Fe-^{15}NO}$ shifts by 7 cm^{-1} to 593 cm^{-1} and ν^{15}_{N-O} shifts by 37 cm^{-1} to 1801 cm^{-1}. For the solvated crystal form, **1·CHCl$_3$**, the 611-cm^{-1} band is assigned to the Fe−NO stretch. This crystal form also exhibits the higher ν_{N-O} frequency of 1868 cm^{-1}. These results are consistent with the structural parameters from the single-crystal X-ray data that show shorter Fe−NO and N−O bond lengths for complex **1·CHCl$_3$**, which has the higher ν_{Fe-NO} and ν_{N-O} frequencies. Figure 5 shows the points for **1** and **1·CHCl$_3$** added to the Fe−N−O frequency correlation plot of Figure 2. Like their six-coordinate thiolate counterparts, these five-coordinate complexes also exhibit a direct correlation between their ν_{Fe-NO} and ν_{N-O} frequencies.

The [Fe(P)NO]$^+$ complex, where P is the dianion of porphine, was chosen as the computational model because of computational limitations brought about by the size of the fully substituted dimeric systems, **1** and **1·CHCl$_3$**. The results from the DFT calculations for the {FeNO}^{6} systems, as well as several [Fe(II)(P)CO] systems, are shown in Tables 1 and 2. These tables contain the relevant bond lengths, bond angles, the scaled (×0.961) harmonic vibrational frequencies, and for comparison, the relevant experimental parameters.

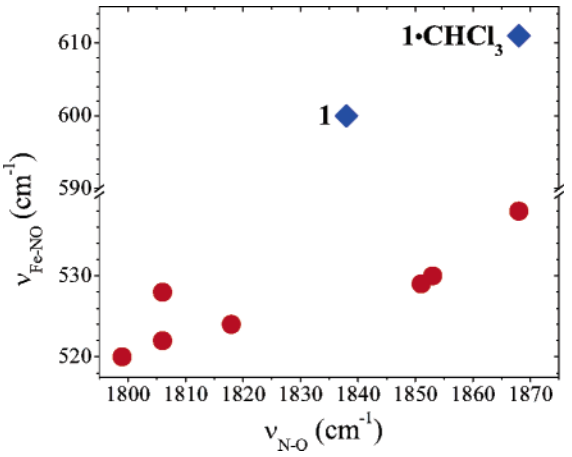

Figure 5. Experimental frequency correlations (ν_{Fe-NO} versus ν_{N-O}) for {FeNO}^{6} systems. Points represent five-coordinate **1** and **1·CHCl$_3$** (◆) and the six-coordinate heme thiolates (●) shown previously in Figure 2.

The DFT-optimized structure for [Fe(P)NO]$^+$ indicates that the Fe−N−O moiety is nearly linear and the structure is essentially C_{4v} symmetric. The structural parameters from the DFT calculation are similar to those from the crystal structures of **1** and **1·CHCl$_3$**. However, there are slight structural differences, including a calculated Fe−NO bond length, R_{Fe-NO}, of 1.614 Å, which is shorter than the experimental values of 1.653 and 1.644 Å for **1** and **1·CHCl$_3$**, respectively. Additionally, the N−O bond is slightly elongated in the DFT-optimized structure (DFT = +0.005 and +0.033 Å). Finally, the essentially linear FeNO moiety calculated by DFT is slightly bent in the crystal structures at ∠FeNO = 173.2° and 176.9°, respectively, for **1** and **1·CHCl$_3$**.

The differences between the DFT-calculated vibrational frequencies and the solid-state experimental values are consistent with the differences between calculated and experimental bond lengths. For ν_{N-O}, the DFT value is 1932 cm^{-1}, while the IR values are 1838 and 1868 cm^{-1}, a reasonable 3−5% difference. For ν_{Fe-NO}, the DFT-calculated value of 682 cm^{-1} is significantly higher than both the rR values of 600 and 611 cm^{-1}. The 12−14% higher DFT value is consistent with the shorter calculated Fe−NO bond length.

In an attempt to clarify the vibrational frequency discrepancies between experiment and theory, several constrained geometry optimizations were performed with the crystal structure values of R_{Fe-NO} and ∠FeNO fixed. The results of these calculations are given in Table 1. For the DFT calculation that mimics **1** (R_{Fe-NO} = 1.653 Å and ∠FeNO = 173.2° held fixed), the ν_{Fe-NO} is 620 cm^{-1}. The energy of this structure is only 0.6 kcal/mol higher than that of the fully optimized structure. The analogous DFT calculation that mimics **1·CHCl$_3$** (R_{Fe-NO} = 1.644 Å and ∠FeNO = 176.9° held fixed) provides a ν_{Fe-NO} of 635 cm^{-1}. This structure is only 0.3 kcal/mol higher in energy than the fully optimized structure. These calculated ν_{Fe-NO} frequencies and their difference are more in line with the experimental

(33) Foresman, J. B.; Frisch, A. *Exploring Chemistry with Electronic Structure Methods*, 2nd ed.; Gaussian: Pittsburgh, PA, 1996.

Table 1. Experimental Bond Lengths, Bond Angles, and Vibrational Stretching Frequencies along with Calculated Values for Five-Coordinate [Fe(P)NO]$^+$ and for Constrained Geometry Optimizations Using B3LYP/6-31G(d)[a]

complex	R_{Fe-NO} (Å)	RN–O (Å)	∠FeNO (deg)	R_{Fe-Np} (Å)	ν_{Fe-NO} (cm^{-1})	ν_{N-O} (cm^{-1})	(references) comments
			Experimental Values				
[Fe(OEP)(NO)]ClO_4 (**1**)	1.653	1.14	173.2	1.994	600	1838	(27) X-ray structure
[Fe(OEP)(NO)]ClO_4·$CHCl_3$ (**1·CHCl$_3$**)	1.644	1.112	176.9	1.994	611	1868	(27) X-ray structure
			Calculated Values (DFT)				
[Fe(P)NO]+	1.614	1.145	180.0	2.006	682	1932	0.0 kcal/mol
R_{Fe-NO} and ∠FeNO fixed at **1·CHCl$_3$** values	1.644 fixed	1.144	176.9 fixed	2.005, 2.008	635	1923	+0.3 kcal/mol
R_{Fe-NO} and ∠FeNO fixed at **1** values	1.653 fixed	1.144	173.2 fixed	2.002, 2.012	620	1919	+0.6 kcal/mol
176.9 (∠Fe−N−O fixed)	1.614	1.145	176.9 fixed	2.004, 2.008	682	1931	+0.04 kcal/mol
173.2 (∠Fe−N−O fixed)	1.615	1.145	173.2 fixed	2.001, 2.011	681	1928	+0.2 kcal/mol
170.0 (∠Fe−N−O fixed)	1.616	1.146	170.0 fixed	1.999, 2.014			+0.5 kcal/mol
165.0 (∠Fe−N−O fixed)	1.619	1.147	165.0 fixed	1.996, 2.017	680	1912	+1.1 kcal/mol
160.0 (∠Fe−N−O fixed)	1.624	1.148	160.0 fixed	1.993, 2.021	677	1897	+1.9 kcal/mol
155.0 (∠Fe−N−O fixed)	1.629	1.150	155.0 fixed	1.990, 2.025	673	1879	+3.0 kcal/mol
150.0 (∠Fe−N−O fixed)	1.637	1.152	150.0 fixed	1.987, 2.028	668	1857	+4.4 kcal/mol

[a] All calculated frequencies have been scaled by 0.961.

Table 2. Calculated Bond Lengths, Bond Angles, and Vibrational Stretching Frequencies for Five-Coordinate {FeNO}^{6} and [Fe^{II}CO] Complexes[a]

complex	R_{Fe-NO} (Å)	R_{N-O} (Å)	∠FeNO (deg)	R_{Fe-Np} (Å)	ν_{Fe-NO} (cm^{-1})	ν_{N-O} (cm^{-1})	comments
				{FeNO}^{6}			
[Fe(P)NO]$^+$	1.614	1.145	180.0	2.006	682	1932	
[Fe(P-β-$(OH)_4$)NO]$^+$	1.612	1.146	179.6	1.998, 2.012	686	1927	
[Fe(P-β-F_8)NO]$^+$	1.617	1.142	180.0	2.002	680	1945	
[Fe(P-β-Cl_8)NO]$^+$	1.619	1.142	180.0	2.011	678	1944	
[Fe(P-β-$(NH_2)_4$)NO]$^+$	1.609	1.148	179.5	2.004, 2.013	690	1920	5.3 kcal/mol higher than meso form
Fe(P-β-(NH_2, $OH)_2$(NO)]$^+$	1.611	1.147	179.0	1.998, 2.012	687	1926	
[Fe(P-*meso*-F_4)NO]$^+$	1.624	1.146	180.0	2.011	674	1922	
[Fe(P-*meso*-Cl_4)NO]$^+$	1.621	1.145	180.0	2.001	677	1930	
[Fe(P-*meso*-$(CH_3)_4$)NO]$^+$	1.615	1.150	180.0	1.980	684	1908	no symmetry imposed
[Fe(P-*meso*-(CH_3, $NH_2)_2$)NO]$^+$	1.627	1.157	179.7	1.990	665 (671)[b]	1867	
[Fe(P-*meso*-$(NH_2)_4$)NO]$^+$	1.657	1.171	150.4	1.978, 2.029	632 (632)[b]	1759	
[Fe(P-*meso*-$(NH_2)_3$)NO]$^+$	1.645	1.164	156.5	1.978, 2.030	645	1806	
[Fe(P-*meso*-$(NH_2)_2$)NO]$^+$	1.626	1.154	179.9	2.005, 2.006	665	1878	
[Fe(P-*meso*-(NH_2))NO]$^+$	1.62	1.149	178.5	2.003, 2.011	678 (672)[b]	1908	
[Fe(P-*meso*-(NH_2, $F)_2$)NO]$^+$	1.636	1.158	165.7	1.998, 2.026	653	1851	
[Fe(P-*meso*-(NH_2, $CH_3)_2$; β-F_4)NO]$^+$	1.634	1.157	167.6	1.978, 2.001			
				[Fe^{II}CO]			
[Fe(II)(P)CO]	1.747	1.152	180.0	2.013	520	2010	
[Fe(P-*meso*-(NH_2))CO]	1.745	1.153	179.9	2.011, 2.014	527 (516)[b]	2005	
[Fe(P-*meso*-$(NH_2)_2$)CO]	1.743	1.154	180.0	2.009	531	1998	
[Fe(P-*meso*-$(NH_2)_4$)CO]	1.742	1.156	180.0	1.999	546	1989	12.5 kcal/mol higher than β-$(NH_2)_4$
[Fe(P-β-$(NH_2)_4$)CO]	1.741	1.154	179.9	2.014, 2.016	527	1998	

[a] All parameters are from B3LYP/6-31G(d) calculations; calculated frequencies have been scaled by 0.961. [b] Mode with smaller Fe−NO stretching contribution.

Raman measurements than those obtained from the unconstrained geometry optimization (Figure 4). This result suggests that the majority of the discrepancy between experimental frequencies and those calculated from optimized gas-phase structures is attributable to lattice-induced distortions of the FeNO moiety. These calculations, and additional constrained geometry (fixed ∠FeNO) optimization calculations listed in Table 1, also reveal that these systems are quite flexible, with very little energy required to perturb their geometries. In fact, bending the linear FeNO unit by 20° (to 160.0°) requires less than 2 kcal/mol, while a bend of 25° (to 155°) requires only 3.0 kcal/mol (RT = 0.6 kcal/mol at 300 K). {FeNO}^{6} structures having ∠FeNO of this magnitude have been observed experimentally in six-coordinate heme proteins and model complexes.[7,34] Interestingly, bending of the FeNO moiety imposes very little out-of-plane distortion of the porphyrin ligand, but does elicit asymmetry in the four Fe−N_P bonds and tilting of the Fe−NO bond with respect to the heme plane (vide infra).

Substituted Models, [Fe(Porph)NO]$^+$. With a starting model that mimics the structural and spectroscopic properties of **1** and **1·CHCl$_3$** in hand, the system was perturbed with the goal of systematically inducing shifts in the ν_{Fe-NO} and ν_{N-O} frequencies to establish the basis of their *direct* correlation. Since complexes **1** and **1·CHCl$_3$** have the same porphyrin periphery, the origin of their different Fe−N−O frequencies must be due to their distinct distal and/or proximal environments. As a means of gaining insight into the intrinsic properties of the {FeNO}^{6} complexes, we have modified the electronic properties of the porphine periphery by introducing a variety of *meso*- and β-pyrrole substituents. Using this approach, it is possible to perform full geometry optimizations and frequency calculations without imposing the arbitrary distance and/or geometry constraints that would be necessary in calculating the effects of

(34) Richter-Addo, G. B.; Wheeler, R. A.; Hixson, L. A.; Chen, L.; Khan, M. A.; Ellison, M. K.; Schulz, C. E.; Scheidt, W. R. *J. Am. Chem. Soc.* **2001**, *123*, 6314−6326.

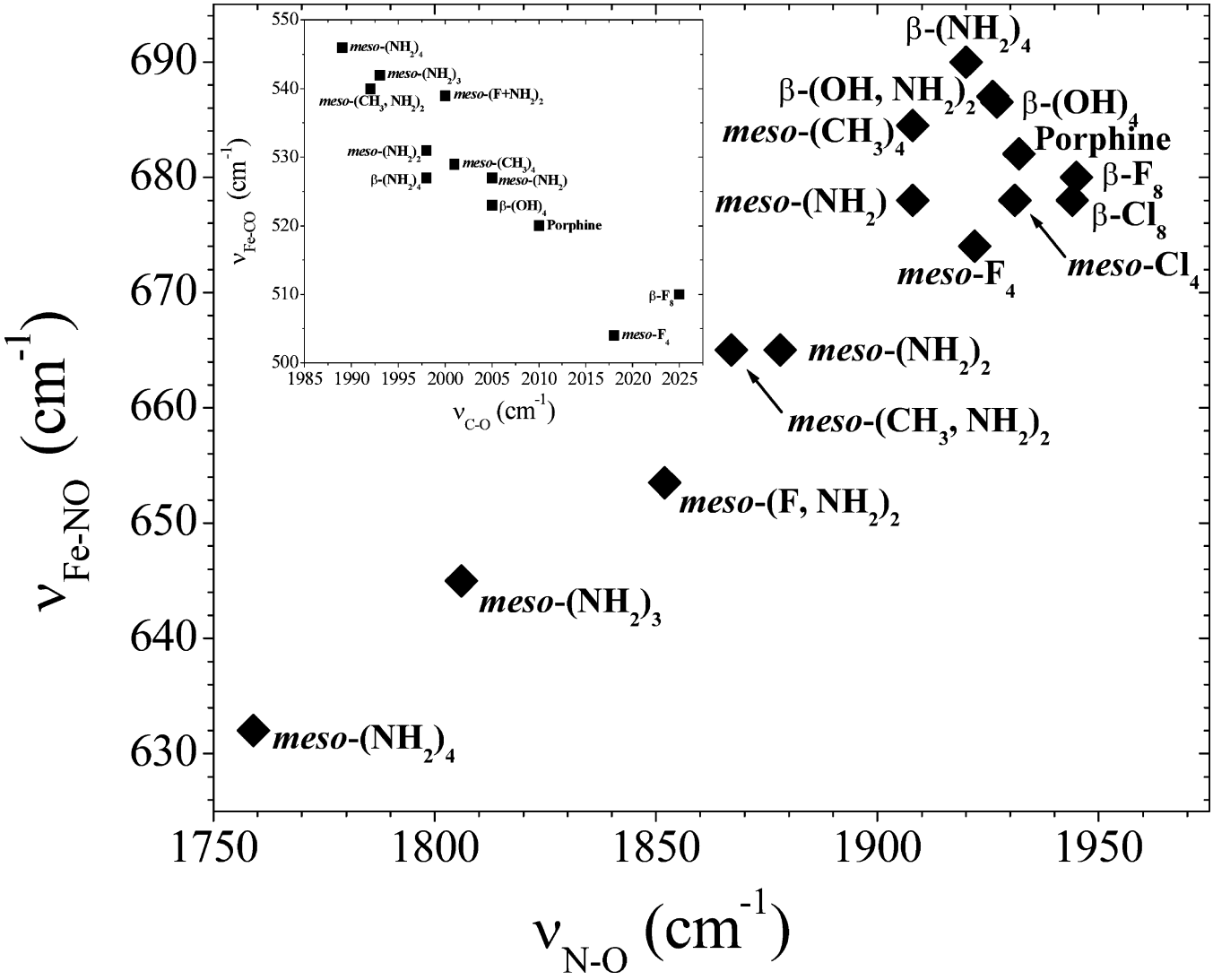

Figure 6. Theoretical frequency correlation (ν_{Fe-NO} versus ν_{NO}) for five-coordinate [Fe(Porph)NO]$^+$ complexes at the B3LYP/6-31G(d) level of theory. Inset: [Fe(Porph)CO] systems.

nonbonded distal interactions. Both the Fe−N−O bond lengths and the frequencies of ν_{Fe-NO} and ν_{N-O} were shown to vary systematically with these substitutions and over a wider range than their Fe(II)CO analogues. As has been observed for Fe(II)CO systems, changes in the electron distribution in the FeNO region of the {FeNO}^{6} complexes should be sensitive to electrostatic interactions with the local environment and/or changes in the electronic properties of the porphyrin ligand.[12,18]

To perturb the [Fe(P)NO]$^+$ system, we have introduced a series of substituents (−NH_2, −OH, −CH_3, −F, and −Cl) in varying numbers at the *meso*- and *β*-pyrrole positions on the porphine ring, providing the basis for a total of 16 calculations. The corresponding variations in Fe−N−O bond lengths, angles, and vibrational frequencies are listed in Table 2, with the corresponding vibrational frequency correlation plot shown in Figure 6. It is evident from this figure that factors affecting the electron density in the FeNO triatomic unit either increase or decrease both ν_{Fe-NO} and ν_{N-O}. Hence, our theoretical model reproduces the *direct* experimental frequency correlation illustrated in Figure 5. Calculations performed on the analogous Fe(II)CO systems reproduce the well-established *inverse* correlation shown in the inset of Figure 6.[35] The *direct* correlation between ν_{Fe-NO} and ν_{N-O} is quite extensive with a range of 58 cm^{-1} for $\Delta\nu_{Fe-NO}$ (632−690 cm^{-1}) and 186 cm^{-1} for $\Delta\nu_{N-O}$ (1759−1945 cm^{-1}). The analogous calculations for Fe(II)CO give values spanning 42 cm^{-1} for $\Delta\nu_{Fe-CO}$ and only 36 cm^{-1} for $\Delta\nu_{C-O}$.

Moreover, an important observation from Figure 6 is that with the progressive addition of electron density at the *meso*-carbon positions (specifically *π*-electron density from −NH_2 or F groups) both ν_{Fe-NO} and ν_{N-O} decrease, suggesting weakening of the entire FeNO unit. For the [Fe(II)(P)CO] complexes with the same *meso*-carbon substitution pattern, the vibrational frequencies follow the expected "back-bonding" pattern of increasing ν_{Fe-CO} and decreasing ν_{C-O}.

Variations in values of ∠FeNO listed in Table 2 raise the question of whether the vibrational frequency data provide an adequate picture of the bonding interactions occurring within the FeNO unit. For the fully optimized [Fe(II)CO] systems, the FeCO unit is always linear (>179°). However, the data in Table 2 reveal that as one progresses from the high to the low end of

(35) Vogel et al.[12] have performed calculations on a smaller subset of the Fe(II)CO systems at the B3LYP/6-31G level of theory.

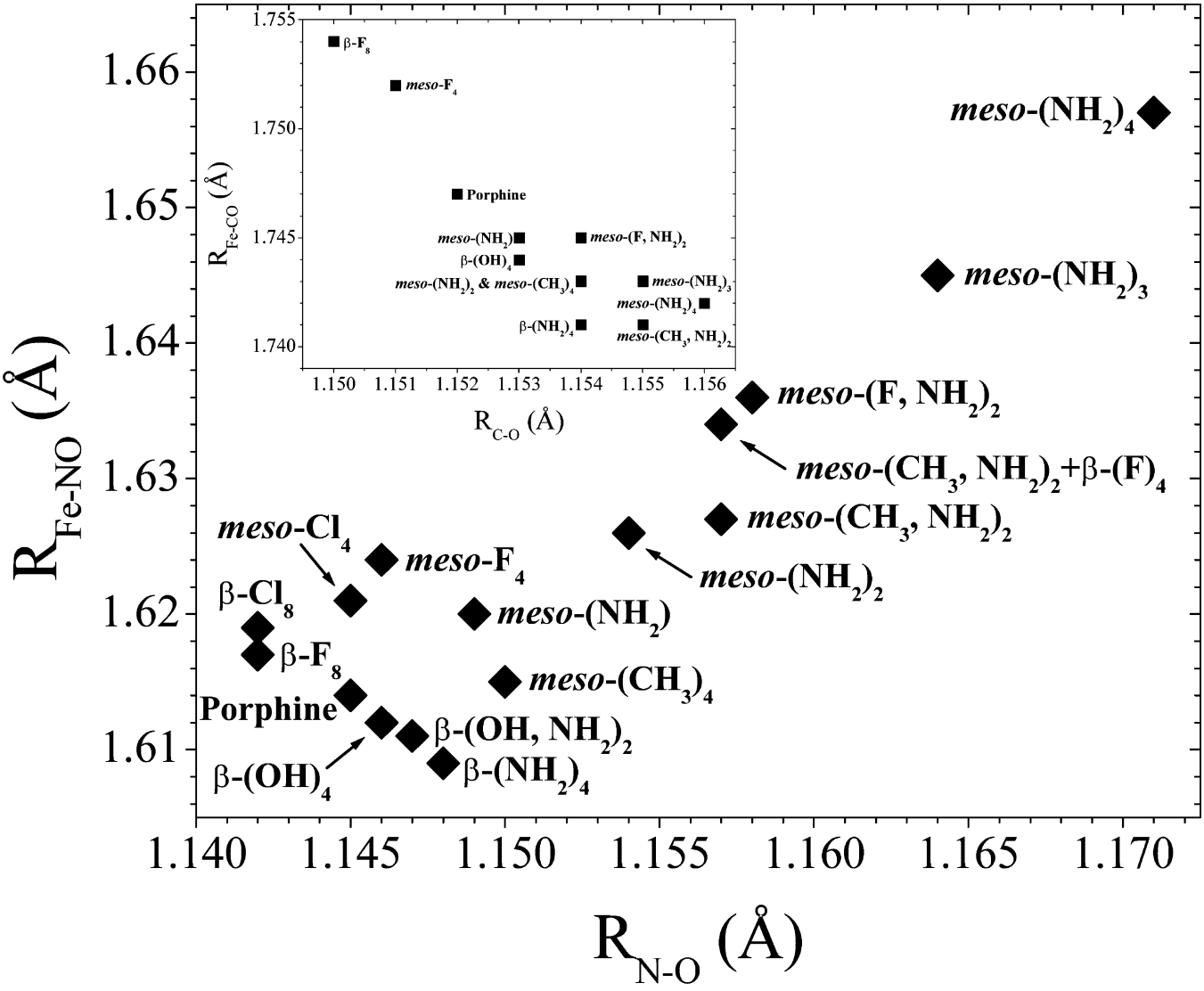

Figure 7. Theoretical bond length correlation (R_{Fe-NO} versus R_{N-O}) for five-coordinate [Fe(Porph)NO]$^+$ complexes at the B3LYP/6-31G(d) level of theory. Inset: analogous [Fe(Porph)CO] complexes.

the {FeNO}^{6} vibrational frequency plot the Fe−N−O unit becomes increasingly bent (150.4° for P-*meso*-$(NH_2)_4$). This raises the possibility that mixing of the Fe−NO stretching and Fe−N−O bending coordinates could complicate interpretation of the *direct* correlation. To address this possibility, we examined the correlation between the Fe−NO and N−O bond lengths, a more unambiguous measure of the Fe−N−O interactions. The plot in Figure 7 clearly shows that, consistent with the vibrational data, R_{Fe-NO} and R_{N-O} increase in concert. Moreover, consistent with the range in vibrational frequencies, the range of bond length differences is substantial with the ΔR_{Fe-NO} values spanning 0.048 Å (1.609−1.657 Å) and ΔR_{N-O} 0.029 Å (1.142−1.171 Å). The corresponding values for Fe(II)CO are $\Delta R_{Fe-CO} = 0.013$ Å and $\Delta R_{C-O} = 0.006$ Å, about one-fourth of the {FeNO}^{6} ranges, and as shown in the inset of Figure 7, R_{Fe-CO} increases while R_{C-O} decreases. Although examination of the vibrational eigenvectors reveals that mixing of internal coordinates does occur to a small extent, the bond length correlation indicates that it is not the origin of the direct frequency correlation and appears to have a negligible impact on it.

As for the experimental Fe−N−O vibrational frequency differences in complexes **1** and **1·CHCl$_3$**, a small basis set, constrained geometry optimization of the unsubstituted dimer $(\mathbf{1})_2$ provides evidence that the porphyrin overlap pattern is not the cause. Since the differences cannot be attributed to different substituents, they must be attributable to either the two molecules of solvent per dimer in **1·CHCl$_3$** or differences in the proximity of the ClO_4^- counterion. At this time we are unable to accurately model the solid-state environment. Consequently, the cause and effect relationship between distal electrostatic fields and the ν_{Fe-NO} versus ν_{N-O} correlation remains unclear. However, the sensitivity of the vibrational correlation to the protein environment is well-established. As with the Fe(II)CO systems, changes in the electron distribution in the Fe−N−O region of the frontier MOs should respond to vicinal electrostatic fields and/or changes in the electronic properties of substituents at the porphine periphery in a similar fashion. Hence, the {FeNO}^{6} moiety is expected to move along the direct correlation line, whether the electron density distribution in the frontier MOs is modulated by bonded or by distal-type nonbonded effects.

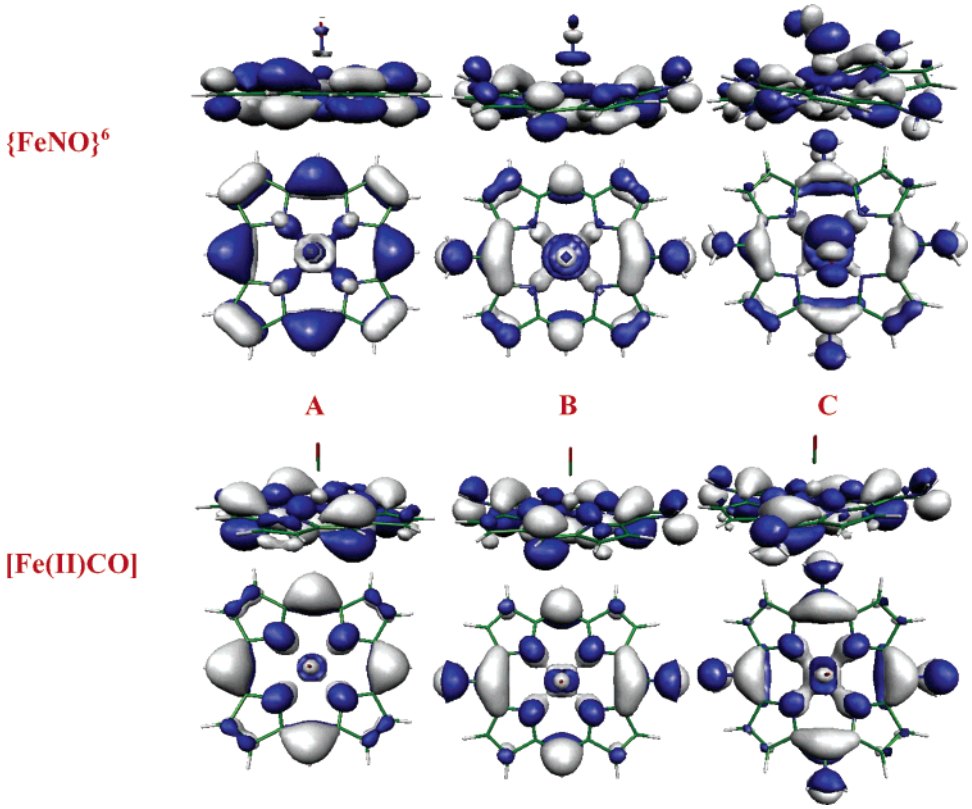

Figure 8. Higher occupied molecular orbitals for {FeNO}^{6} (top) and [Fe(II)CO] (bottom) complexes. (A) Porphine (HOMO-1). (B) *meso*-$(NH_2)_2$ (HOMO). (C) *meso*-$(NH_2)_4$ (HOMO).

Discussion

Together with published studies on other {FeNO}^{6} systems, the experimental and computational results presented here constitute a self-consistent description of the sensitivity of bonding in the FeNO moiety to both intramolecular and environmental factors. Furthermore, the bonding description set forth herein provides insight into reactivities of the coordinated NO and the Fe−NO bond in {FeNO}^{6} porphyrinates. Although this bonding description has grown out of the complementarity between experiment and calculation, the following discussion is composed in terms of predictions based on computational results and the consistency of those predictions with experimental results presented here and with others from the literature.

Orbital Interactions Responsible for the Direct Correlation. The highest occupied MO that places electron density on the NO ligand in the calculated {FeNO}^{6} complexes is either the HOMO or the HOMO-1 (HOMO/HOMO-1), depending upon the peripheral substituent pattern (see top of Figure 8). This MO is largely σ-antibonding with respect to the entire Fe−N−O triatomic unit. This result suggests that any intramolecular or nonbonded environmental factors that polarize the electron density of this MO toward the FeNO core will increase the antibonding character of the orbital with respect to the FeNO moiety. This would be predicted to lengthen both the Fe−NO and N−O bonds and decrease their stretching frequencies. Conversely, factors that polarize electron density away from the FeNO moiety would be expected to shorten the Fe−NO and N−O bonds and increase the frequencies of their stretching vibrations. This analysis is consistent with two lines of experimental evidence. First, the ν_{Fe-NO} and ν_{N-O} stretching frequencies of **1** and **1·CHCl$_3$** shift in the same direction in response to change in the FeNO environment due to the effects of the solvent molecule in the crystal lattice. Moreover, the higher frequencies are observed in the complex having the shortest distance (most repulsive interaction) between coordinated NO and the perchlorate counterion. The second line of evidence in support of this theoretical prediction is that a series of {FeNO}^{6} porphyrinates with trans thiolate ligands and a range of distal environments exhibit a *direct* correlation between the strengths of the Fe−NO and N−O bonds (as reported by the respective bond stretching frequencies).[21,22]

To help provide insight into the orbital interactions responsible for the *direct* correlation of frequencies in the five-coordinate {FeNO}^{6} systems and the lack thereof in the [Fe(II)CO] systems, a description of the frontier orbitals is in order. The distribution of electron density within these highest-energy occupied orbitals is more responsive to change in chemical structure of the tetrapyrrole ligand and its environment than the lower-energy MOs. This sensitivity is a transducer for influence of structure and environment on the reactivity of the complex. It can be difficult to distinguish small variations in electron density distributions within large and highly delocalized molecular orbitals. However, those shown in Figure 8[36] reveal pronounced differences between analogous MOs of the isoelectronic [Fe(Porph)NO]$^+$ (top) and [Fe(Porph)CO] (bottom) complexes. These differences lie in the electron density on the XO ligand, and a series of examples will illustrate this point. Consider first the simplest case of porphine. It is clear from Figure 8A (top: HOMO-1 for [Fe(P)NO]$^+$, bottom: HOMO-1

(36) All MO figures (isosurfaces) were produced with the program MOLEKEL version 4.2. Swiss National Supercomputing Centre Home Page. http://www.cscs.ch/molekel/. Portman, S.; Lüthi, H. P. *Chimia* **2000**, *54*, 766−770.

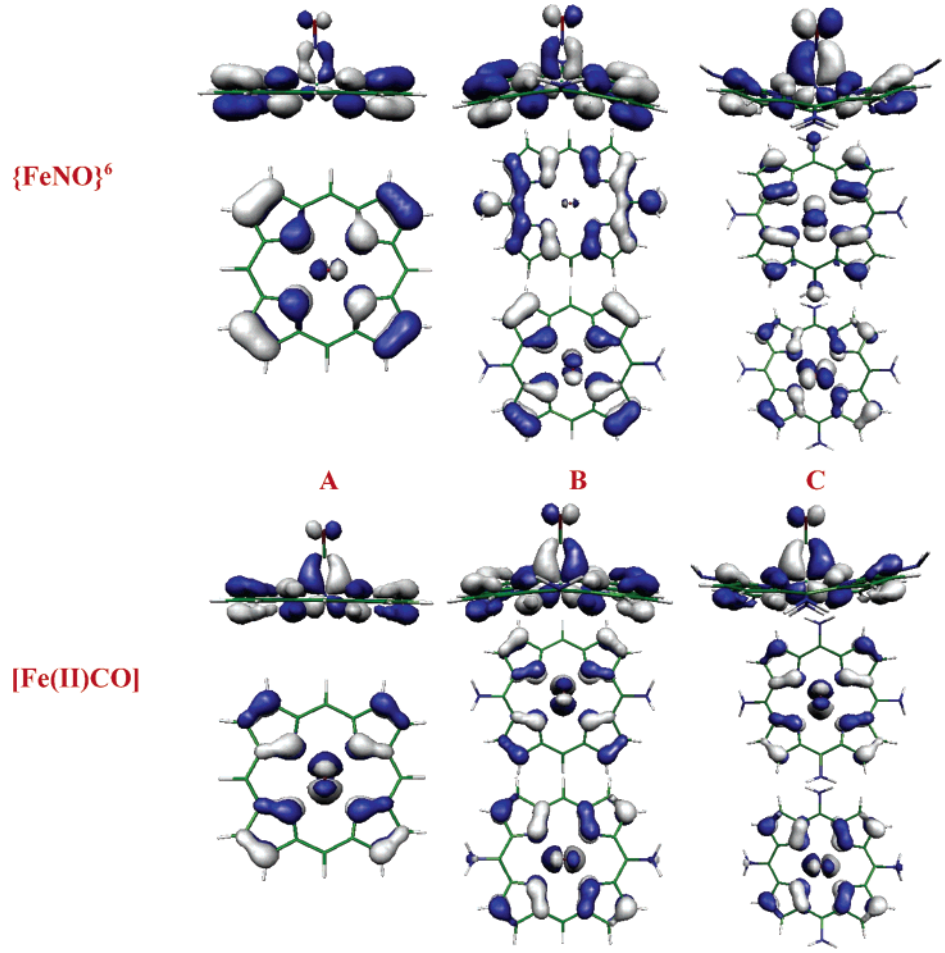

Figure 9. HOMO-(2,3) for $\{FeNO\}^6$ (top) and [Fe(II)CO] (bottom) complexes. (A) Porphine. (B) *meso*-$(NH_2)_2$. (C) *meso*-$(NH_2)_4$.

[Fe(P)CO]) that the HOMO-1 of $[Fe(P)NO]^+$ is σ-antibonding throughout the FeNO triatomic unit. On the other hand, the HOMO-1 of [Fe(P)CO] is nonbonding with respect to FeCO. Next, consider the [Fe(P-*meso*-$(NH_2)_2$)NO]$^+$ and [Fe(P-*meso*-$(NH_2)_2$)CO] complexes, shown in Figure 8B. These complexes have similar geometries containing linear Fe−X−O units, and both are approximately in the middle of their respective frequency and bond length correlation plots. In this case, the HOMO of [Fe(P-*meso*-$(NH_2)_2$)NO]$^+$ is entirely σ-antibonding with respect to FeNO, while the HOMO of [Fe(P-*meso*-$(NH_2)_2$)-CO] is once again devoid of any FeCO interactions. Also, the increased σ-antibonding electron density in the [Fe(P-*meso*-$(NH_2)_2$)NO]$^+$ complex, with respect to $[Fe(P)NO]^+$, is consistent with longer Fe−N−O bonds and lower Fe−N−O frequencies. Finally, a complex at the low-frequency (long bond) extreme of the correlation, [Fe(P-*meso*-$(NH_2)_4$)NO]$^+$, is shown in Figure 8C. The orbital analysis for this situation is complicated by the fact that the FeNO unit is bent ($\angle$FeNO = 150.4°). Nevertheless, it is clear from the top of Figure 8C that, even at this extreme of the correlation, the HOMO is strongly σ-antibonding with respect to Fe−N−O. Once again, the HOMO in the [Fe(P-*meso*-$(NH_2)_4$)CO] complex shows no signs of Fe−C−O interactions. This set of orbitals shows that through functionalization of the porphyrin periphery at meso positions, σ-antibonding electron density builds up in the FeNO core, thereby decreasing the strengths of the Fe−NO and N−O bonds in unison.

While the molecular orbitals in Figure 8 qualitatively account for the observed Fe−N−O bond-strength behavior of the $\{FeNO\}^6$ systems, they provide no insight into (or evidence for) the orbital interactions that account for the inverse correlation of the Fe(II)CO systems. For these interactions, we must examine lower-energy MOs. These MOs are shown for the series of $\{FeNO\}^6$ and [Fe(II)CO] complexes at the top and bottom of Figure 9, respectively. These orbitals comprise the HOMO-(2,3) pair. For complexes of C_{4v} symmetry (Figure 9A), the HOMO-(2,3) orbitals are degenerate. When the fourfold symmetry is broken by distortion of the FeXO moiety or peripheral substitution pattern, this degeneracy is lifted. In these cases (Figure 9B,C), both orbitals are shown. The character of this entire set of MOs is π-bonding with respect to Fe−XO and π-antibonding with respect to X−O, for both the $\{FeNO\}^6$ and [Fe(II)CO] series of complexes. If the FeXO electron density in these MOs is the most responsive to environmental changes (i.e., if they are the highest-energy MOs with electron density on FeXO), then any structural or environmental perturbation that polarizes the electron density distribution toward the FeXO core will increase the Fe−XO bond order while decreasing that of X−O. Thus, a shortening of Fe−XO along with an increase in its stretching frequency would be predicted to occur in concert with a lengthening of the X−O bond and a decrease in its stretching frequency. Conversely, factors that polarize electron density away from the FeXO moiety would be expected to

lengthen the Fe−XO and shorten the X−O bonds with the respective decrease and increase of their vibrational stretching frequencies.

The highest occupied MOs that place electron density on the CO ligand in the calculated [Fe(II)(P)CO] complexes are the HOMO-(2,3) pair shown in the bottom of Figure 9. Thus, the responsiveness of electron density distribution in these orbitals is expected to dominate the relative changes in the Fe−CO and C−O bond strengths and vibrational frequencies inversely upon changing the structure or environment of the complex. This analysis is consistent with the large body of data for the Fe(II)CO systems. In fact, these occupied MOs are responsible for the behavior so commonly rationalized within the "back-bonding" model (Figure 1A).[37] However, how these π-orbitals influence the {FeNO}^{6} systems remains to be explained.

Figure 9A shows that both the {FeNO}^{6}− and [Fe(II)CO]− porphine complexes exhibit a very similar and nearly degenerate HOMO-(2,3) pair. Both members of this pair are π-bonding with respect to Fe-XO *and* π-antibonding with respect to X−O. This is also true for the [Fe(P-*meso*-$(NH_2)_2$)NO]$^+$ and [Fe(P-*meso*-$(NH_2)_2$)CO] complexes whose orbitals are shown in Figure 9B. The {FeNO}^{6} complex at the low-frequency (long bond) extreme of the correlation, [Fe(P-*meso*-$(NH_2)_4$)NO]$^+$, is shown in Figure 9C. The orbital analysis for this situation is again complicated by the bent FeNO unit (150.4°). Nevertheless, it is clear that in the lower-lying HOMO-(2,3) pair, one is strongly Fe−XO π-bonding and X−O π-antibonding while the character of the other is skewed because of the bend.

For the [Fe(II)CO] complexes, the series of π MOs at the botton of Figure 9 shows a clear and qualitatively consistent picture of the orbital interactions that are responsible for the *inverse* stretching frequency correlation in Fe(II)CO porphyrin systems. In these complexes, the correlated frequency shifts were induced by systematic in silico modification of the porphyrin periphery, which affects Fe−C−O bonding via highly delocalized MOs. The top of Figure 9 shows that these π MOs are very similar for the {FeNO}^{6} complexes, albeit with a more uniform electron density distribution within the FeNO moiety (i.e., more covalent interactions). The contribution of these π MOs to the *direct* vibrational frequency correlation of the {FeNO}^{6} systems is neither zero nor negligible. As stated earlier, the ranges of the *direct* correlation are much larger than those of the *inverse* correlation ($\Delta\nu_{N-O} = 186$ cm^{-1}, 10.0% of the mean and $\Delta\nu_{C-O} = 36$ cm^{-1}, 1.8% of the mean; see Figure 6). The higher-energy and more polarizable HOMO/HOMO-1 (Figure 8) undoubtedly accounts for most of the range of the *direct* ν_{Fe-NO} versus ν_{N-O} frequency correlation. However, the N−O π* character of the HOMO-(2,3) MOs adds to the N−O bond weakening as FeNO becomes increasingly electron-rich. These combined effects appear to be responsible for the disproportionately large range of ν_{N-O} frequencies relative to ν_{C-O}. Moreover, the sensitivity of Fe−NO π-bonding due to the substituent effects on electron density distribution in HOMO-(2,3) is overwhelmed by the larger polarizability of the higher-energy HOMO/HOMO-1 with its Fe−N−O σ* character. This analysis provides a consistent picture of the *direct* stretching

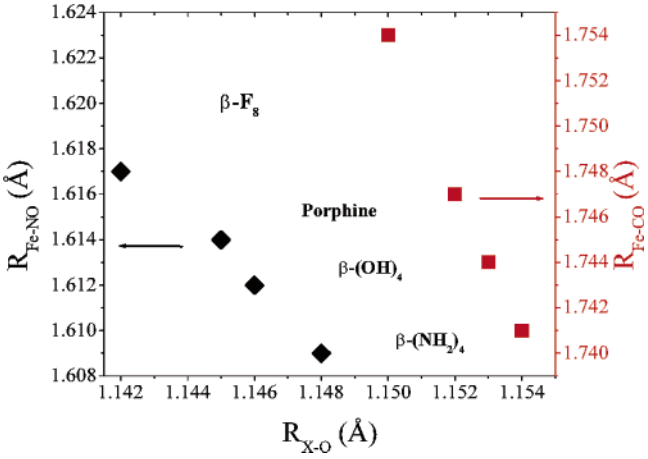

Figure 10. Theoretical bond length correlation (R_{Fe-XO} versus R_{X-O}) for five-coordinate β-pyrrole-substituted [Fe(Porph)NO]$^+$ (◆) and [Fe(Porph)-CO] (■) systems at the B3LYP/6-31G(d) level of theory.

frequency correlation (Figure 6) for the meso-substituted porphyrins listed in Table 2. However, when the same substituents are placed in β-pyrrole positions, the FeNO behavior changes.

An Inverse Correlation for {FeNO}^{6}? An interesting nuance of this study is revealed by indirect correlations of ν_{Fe-NO} with ν_{N-O} and of R_{Fe-NO} with R_{N-O} for a subset of the {FeNO}^{6} complexes. These calculated indirect correlations are consistent with a recent report containing {FeNO}^{6} frequencies for reconstituted P450nor-NO that show an indirect ν_{Fe-NO} vs ν_{N-O} correlation.[38] Figures 6 and 7 and Table 2 show that, among the {FeNO}^{6} complexes, those in which only the β-pyrrole substituents are varied exhibit ν_{Fe-NO} and ν_{N-O} sensitivities distinct from the direct correlation of their meso-substituted counterparts. The points for the β-pyrrole-substituted complexes are clustered around the unsubstituted porphine complex in both the frequency and bond-length correlation plots. Moreover, their ν_{Fe-NO} and ν_{N-O} frequencies and bond lengths are *inversely* correlated. The influence of changes in the β-pyrrole substituents on the relationship between Fe−XO and X−O bond strengths is comparable in the {FeNO}^{6} and [Fe(II)CO] complexes. This is shown quite clearly by their bond-length correlations in Figure 10.[39] The points in Figure 10 comprise a subset of the data in Figure 7. They are plotted on the same *x* axis with the same *y* range, the latter being offset by 0.131 Å for ease of viewing. The similar slopes and ranges of the two correlations in Figure 10 suggested that their fundamental origins might also be similar.

Comparison of analogous occupied molecular orbitals of *meso*- and β-pyrrole-substituted porphyrins indeed supports the notion that the indirect correlations in Figure 10 are attributable to analogous electronic effects. For the β-pyrrole-substituted {FeNO}^{6} complexes, the HOMO-1, which is completely σ-antibonding with respect to Fe−N−O in the meso-substituted complexes, has very little electron density on the coordinated NO ligand (Figure 11). Additionally, this FeNO σ* electron density appears mostly independent of the extent and nature of β-pyrrole substitution. Because the Fe−N−O σ* character of

(37) Hereinafter, the term back-bonding is not used. This is to help prevent the confusion of electron density distribution within a given molecular orbital and the origin of the electrons that occupy them. This is done as part of an effort to focus attention on where the electrons *are* in the complex and how their distributions relate to the structure, bonding, and reactivity thereof.

(38) Singh, U. P.; Obayashi, E.; Takahashi, S.; Iizuka, T.; Hirofumi, S.; Shiro, Y. *Biochim. Biophys. Acta* **1998**, *1384*, 103−111.

(39) The same effect is observed for the vibrational frequencies; however, they do not fit neatly on the same *X*-axis.

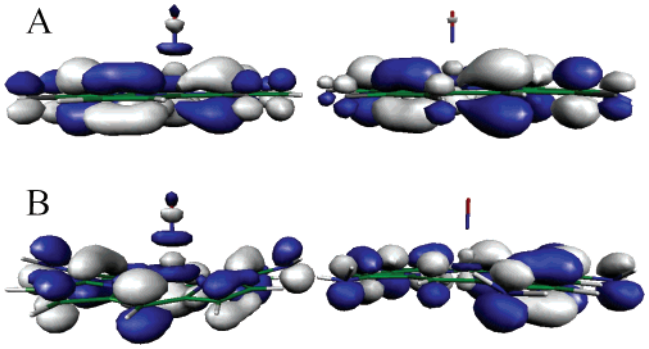

Figure 11. HOMO or HOMO-1 for {FeNO}^{6} complexes. (A) [Fe(P-*meso*-F_4)NO]$^+$ (HOMO) and [Fe(P-β-F_8)NO]$^+$ (HOMO-1). (B) [Fe(P-*meso*-$(NH_2)_2$)NO]$^+$ (HOMO) and [Fe(P-β-$(NH_2)_4$)NO]$^+$ (HOMO-1).

HOMO-1 is essentially insensitive to variation in the β-pyrrole substituents, the electron density distribution in the MOs having Fe−NO π/N−O π* character becomes the determining factor in the sensitivities of the Fe−NO and N−O bond strengths. Consequently, the direct relationship between Fe−NO and N−O bonding is essentially unresponsive to variations in the β-pyrrole substituents. Additionally, and no less importantly, for the [Fe(P-β-$(NH_2)_4$)NO]$^+$ complex the HOMO has a small amount of electron density on the FeNO moiety (not shown), and it is also of Fe−NO π/N−O π* character. Hence, the HOMO (in addition to HOMO-(2,3)) contributes to the *inverse* sensitivities of the Fe−NO and N−O bond strengths to changes in β-pyrrole substituents.

The calculated effects of β-pyrrole variation are consistent with reported ν_{Fe-NO} and ν_{N-O} frequencies for cytochrome P450nor-NO from the denitrifying fungus *Fusarium oxysporum* reconstituted with proto-, meso-, and deuteroheme.[38] In that study, the environmental factors were held constant by using the same protein matrix to host three hemes having different β-pyrrole (2,4) substituents. Plots of the frequencies reported for the corresponding {FeNO}^{6} and [Fe(II)CO] complexes reveal *inverse* correlations over approximately the same ranges in frequency for proto-, meso-, and deuteroheme. Singh, et al.[38] concluded that the small frequency ranges of the ν_{Fe-NO} and ν_{N-O} bands were not significant and that the changes in the porphyrin 2,4 substituents do not influence the Fe−NO bond. This is a reasonable conclusion, given that the reported frequency differences are on the order of the uncertainty with which Raman frequencies can typically be determined. However, plots of ν_{Fe-NO} versus ν_{N-O} and ν_{Fe-CO} versus ν_{C-O} both show inverse correlations with similar frequency ranges. The consistency of this behavior with the calculated ranges of the inverse correlations shown in Figure 10 suggests that, although it is small, the experimental correlation may be real. These results suggest that an inverse relationship between the Fe−NO and the N−O bond strengths can only be observed for variations in the β-pyrrole substituents when the heme environment remains otherwise unchanged.

Charge Analysis. Additional theoretical evidence to support the different FeNO and FeCO sensitivities to meso- and β-substituents is found in a partial-charge analysis, performed using the natural population analysis (NPA) scheme.[40] The charge analysis results are shown graphically in Figure 12 as partial charge on Fe (q_{Fe}) versus partial charge on NO (q_{NO}). This plot reveals that four *meso*-F atoms actually increase the electron density associated with the Fe−N−O core, thereby decreasing the positive charge on Fe and NO in concert. Figure 12 shows that four *meso*-F atoms have approximately the same effect on FeNO charge as a single *meso*-NH_2 group. Conversely, Figure 12 shows that the Fe centers and NO ligands in [Fe(P-β-F_8)NO]$^+$ and [Fe(P-β-$(NH_2)_4$)NO]$^+$ exhibit an *inverse* charge relationship. These partial charge data are consistent with all the vibrational frequency and bond length data presented in Figures 6 and 7.

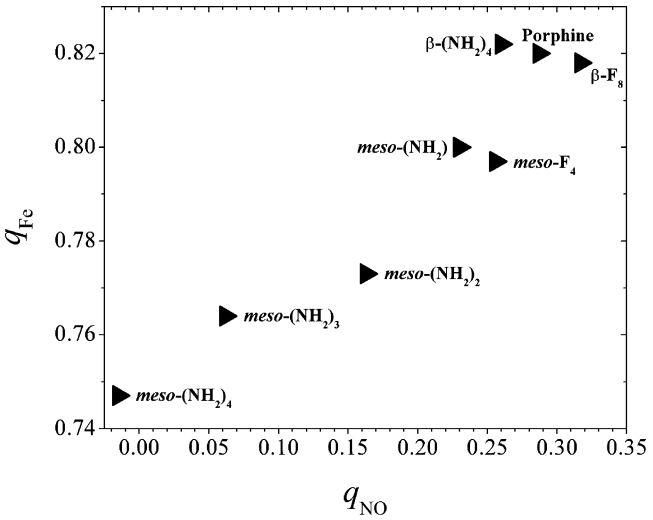

Figure 12. Partial charge correlation (q_{Fe} versus q_{NO}) for five-coordinate [Fe(Porph)NO]$^+$ complexes at the B3LYP/6-31G(d) (NPA) level of theory.

Other Structural Sensitivities to Peripheral Substituents. Examination of Figures 8 and 9 also reveals several interesting structural differences of the porphyrin macrocycle. As the total electron donor (especially π donor) ability of the meso substituents on porphine increases, there are two marked changes in the HOMO or HOMO-1. First, electron density is increasingly redistributed toward the first coordination sphere of the iron. Second, the porphyrin ring adopts an increasingly ruffled conformation. Given the widespread interest in out-of-plane porphyrin deformations and their roles in heme protein function, this trend warrants comment. Because our calculations were carried out on isolated gas-phase ions and molecules with the only axial ligands being NO or CO, ruffling is unlikely to be attributable to steric interactions between the porphyrin and the axial ligand. Another possible driving force for ruffling is electronic stabilization by bonding interactions that can only appear upon symmetry lowering along the ruffling coordinate. Such stabilization has been seen in six-coordinate, low-spin ferric porphyrins having π-accepting axial ligands such as alkylisocyanides.[41] This stabilization derives from a bonding interaction between the d_{xy} and the a_{2u} (under D_{4h} symmetry) porphyrin orbital that becomes symmetry-allowed in a D_{2h} (ruffled) complex. However, careful examination of the frontier MOs of the five-coordinate [Fe(Porph)NO]$^+$ complexes (down to HOMO-10) revealed no such stabilizing interactions. Hence,

(40) Reed, A. E.; Weinstock, R. B.; Weinhold, F. *J. Chem. Phys.* **1985**, *83*, 739−746. The NPA scheme used was the Gaussian 98 implementation, NBO version 3.1. Glendening, A. D.; Reed, A. E.; Carpenter, J. E.; Weinhold, F. University of Wisconsin, Madison, 2002.

(41) (a) Walker, F. A.; Nasri, H.; Turowska-Tyrk, I.; Mohanrao, K.; Watson, C. T.; Shokhirev, N. V.; Debrunner, P. G.; Scheidt, W. R. *J. Am. Chem. Soc.* **1996**, *118*, 12109−12118. (b) Walker, F. A. *Coord. Chem. Rev.* **1999**, *185*−*186*, 471−534.

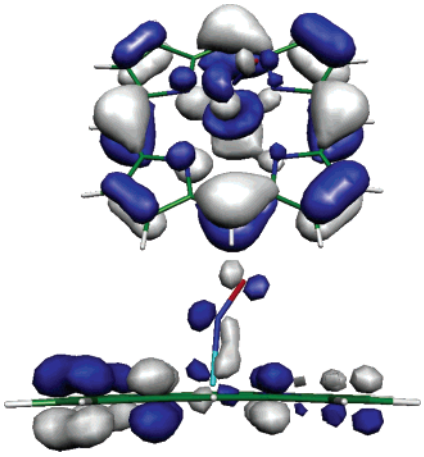

Figure 13. Molecular orbitals relevant to Fe−N−O bending and Fe−$N_{pyrrole}$ asymmetry. Geometry-minimized for a fixed FeNO angle of 150° in [Fe(P)NO]$^+$. HOMO-1 (top) and HOMO-3 (bottom).

the most likely driving force for ruffling is the relief of steric interactions involving the peripheral porphyrin substituents. This is confirmed upon comparison of the extent of ruffling in [Fe(P)NO]$^+$, [Fe(P-*meso*-F_4)NO]$^+$, [Fe(P-*meso*-Cl_4)NO]$^+$, [Fe(P-*meso*-$(CH_3)_4$)NO]$^+$, [Fe(P-*meso*-$(NH_2)_2$)NO]$^+$, and [Fe(P-*meso*-$(NH_2)_4$)NO]$^+$, which reveals that ruffling in these structures is driven by interactions between meso substituents and β-pyrrole hydrogen atoms. The extent of ruffling for the ferrous CO complexes depends on meso substituents in a manner similar to the {FeNO}^{6} complexes. Moreover, by constraining the NO to a bent geometry in [Fe(P)NO]$^+$, the optimized porphine conformation is nearly flat.

Examination of Figure 8 and Table 2 also reveals that significant increases in FeNO electron density due to meso substitution elicit bending of the FeNO moiety. This is accompanied by the appearance of asymmetry in the Fe−$N_{pyrrole}$ core. The data in Table 1 show that this asymmetry tracks inversely with ∠FeNO. There appear to be two MOs relevant to FeNO bending and equatorial asymmetry; they are most easily identified in the constrained geometry optimization of [Fe(P)NO]$^+$ with ∠FeNO frozen at 150° and are shown in Figure 13. The top orbital, HOMO-1, comprises a slanted Fe-centered d_{z^2} contribution with its bottom lobe involved in a bonding interaction with the two $N_{pyrrole}$ atoms closest to the terminal oxygen atom of NO. This interaction elicits equatorial asymmetry and is likely the reason for Fe−$N_{pyrrole}$ bonds being shorter on the side of the Fe−N_p core toward which the NO bends. As for the FeNO bend itself, Tables 1 and 2 reveal that the Fe−NO bond is weakened, as gauged by its increased length, either upon introduction of π electron density at the *meso*-carbons of the porphine ligand or with enforced bending of the FeNO unit. This loss in Fe−NO bond order is partially compensated by bending of the FeNO unit, which facilitates two bonding interactions that might otherwise be weak or nonexistent in a linear FeNO unit having a long Fe−NO bond. The first is illustrated by the bottom MO of Figure 13, which shows HOMO-3 for [Fe(P)NO]$^+$ with ∠FeNO constrained at 150°. The Fe d_π/NO π^* interaction in the FeNO plane shows that the bend facilitates significant Fe−NO bonding, even for a long Fe−NO bond. Further stabilization is provided by a bonding interaction, albeit small, between the electron densities on Fe (d_{z^2}) and the oxygen atom of N−O; this can be seen on the top of Figure 8C, where it is illustrated for [Fe(P-*meso*-$(NH_2)_4$)NO]$^+$.

The term "slanted" has been used deliberately to describe the orientation of the d_{z^2} contribution to the HOMO and HOMO-1 in Figures 8C and 13, respectively. The reason for introduction of this terminology is to distinguish between the Fe(d_{z^2}) angle with respect to the normal to the mean porphyrin plane and that of the Fe−N−O tilt, which are of *opposite* sign. This seemingly counterintuitive situation appears necessary to accommodate both the equatorial asymmetry and the Fe d_π/NO π^* bonding interaction upon FeNO bending. Interestingly, this interplay between FeNO bending, Fe−NO tilting, d_{z^2} slanting, and Fe−$N_{pyrrole}$ asymmetry appears to be general. Consistent with the negligible Fe−N−O σ^* character of HOMO-1 in [Fe(P-β-$(NH_2)_4$)NO]$^+$, there is little electronic driving force for bending of the {FeNO}^{6} core. Consequently, the FeNO unit is only slightly distorted, and the corresponding Fe−$N_{pyrrole}$ asymmetry is much smaller ($\Delta r \simeq 0.01$ Å) than that in [Fe(P-*meso*-$(NH_2)_4$)NO]$^+$ ($\Delta r \simeq 0.05$ Å). A similar relationship between Fe−N−O tilt and equatorial asymmetry has been observed in {FeNO}^{7}.[42,43]

Fe−N−O Bonding and Reactivity of Coordinated NO. The results presented here have interesting implications in understanding the relationship between structure and reactivity of the {FeNO}^{6} moiety. This is illustrated by considering the NO adduct of nitrophorin 4 (NP4−NO), which contains a {FeNO}^{6} heme that is both labile with regard to NO release and unreactive toward reductive nitrosylation. A 1.08 Å crystal structure of NP4−NO from *R. prolixus* shows ∠FeNO = 155°, albeit with no apparent equatorial asymmetry.[7] A space-filling view of the distal heme pocket in this structure suggests that the FeNO bend occurs at least in part as a result of steric interactions with the side chains of leucines 123, 130, and 133. Given that one of the major roles of this protein is NO delivery, the results reported here suggest that the inverse relationship between Fe−NO bond strength and ∠FeNO in {FeNO}^{6} systems might be the basis of a cause-and-effect relationship between the bent NP4−NO structure and its facile release of NO. Additionally, concentration of electron density on the bent FeNO unit is apt to make it less susceptible to nucleophilic attack by water or hydroxide. Since this is the rate-determining step in reductive nitrosylation,[28,44] the electron-rich {FeNO}^{6} is much less susceptible to release of HNO_2 with subsequent formation of the more stable {FeNO}^{7} complex. Hence, the basis of the direct correlations shown in Figures 6 and 7 may also be the basis for both redox stability and NO lability of NP4−NO.

While the relationships between ∠FeNO, Fe−NO bond length, and electrophilicity of the coordinated NO established here for the five-coordinate complexes suggest an attractive model for the lability and redox stability of NP4−NO, it should be borne in mind that NP4−NO contains a six-coordinate heme with an imidazole ligand trans to NO. The heme also exhibits significant out-of-plane distortion along the ruffling (−0.854 Å) and saddling (0.333 Å) coordinates.[7] At this time, the vibrational frequency data for imidazole-bound {FeNO}^{6} hemes

(42) Ghosh, A.; Wondimagegn, T. *J. Am. Chem. Soc.* **2000**, *122*, 8101−8102.
(43) Scheidt, W. R.; Ellison, M. K. *Acc. Chem. Res.* **1999**, *32*, 350−359.
(44) (a) Hoshino, M.; Maeda, M.; Konishi, R.; Seki, H.; Ford, P. C. *J. Am. Chem. Soc.* **1996**, *118*, 5702−5707. (b) Addison, A. W.; Stephanos, J. J. *Biochemistry* **1986**, *25*, 4104−4113. (c) Hoshino, M.; Ozawa, K.; Seki, H.; Ford, P. C. *J. Am. Chem. Soc.* **1993**, *115*, 9568−9575.

are sparse and equivocal with regard to a correlation between the sensitivities of Fe−NO and N−O bond strengths to electronic and environmental factors. However, recent computational results (Linder and Rodgers, manuscript submitted) reveal a correlation similar to that reported here. As more experimental data become available for imidazole-bound {FeNO}^{6} complexes, it will be interesting to learn whether Fe−NO bond length and k_{off} or K_d actually track inversely with ∠FeNO.

Summary and Conclusions

The computational and experimental results discussed above suggest that electron density in the FeNO moiety is responsive to bonded and nonbonded interactions between the FeNO unit and its immediate environment and/or the porphyrin ligand. These modulations are affected through influence over electron density distribution in three of the higher occupied porphyrin π MOs. The highest-energy orbital, which is the HOMO/HOMO-1 (Figure 8), has σ^* character with respect to Fe−N−O, whereas the lower-energy MOs, HOMO-(2,3), have Fe−NO π/N−O π^* character (Figure 9). Because HOMO/HOMO-1 is the more polarizable of the three, the sensitivity of its electron density distribution to bonded and nonbonded interactions is expected to be greater than that of the other two MOs. Hence, effects on HOMO/HOMO-1 will dominate changes in FeNO bonding. Thus, changes in the electrostatic environment around the bound NO ligand are manifested in strengthening or weakening of both the Fe−NO and N−O bonds. This parallel effect on these bonds is revealed in the direct correlation between indicators of the bond strengths, ν_{Fe-NO} and ν_{N-O} frequencies, and Fe−N−O bond lengths. This direct correlation in bond-strength sensitivity is borne out experimentally for **1** and **1·CHCl$_3$** and for a group of thiolate-bound heme enzymes, which represent a range of protein environments for the same {FeNO}^{6} complex (Figure 5).

The changes in Fe−NO and N−O bond strengths in response to structural and electronic modification of the porphyrin ligand depend on which positions around the porphyrin periphery are modified. Changes in functional groups at meso positions modulate FeNO electron density in the HOMO/HOMO-1, which causes the bonding changes to be directly correlated, as shown in Figures 6 and 7. This is a large effect that dominates the relationship between the Fe−NO and N−O bond strengths and causes ν_{Fe-NO} and ν_{N-O} to vary over a wide range. Changes at the β-pyrrole positions preferentially modulate FeNO electron density in the HOMO-(2,3) pair. This influence causes changes in FeNO bonding along the indirect correlation shown in Figure 10, which is much smaller in magnitude than the direct effects. These results are consistent with the direct ν_{Fe-NO} versus ν_{N-O} frequency correlation observed for {FeNO}^{6} protoheme in a range of protein environments,[21,22] and why an inverse correlation is observed for a series of hemes having different β-pyrrole substituents in the same protein.[38]

The results presented here along with data from the literature constitute a self-consistent view of the bonding in {FeNO}^{6} porphyrinates. Furthermore, the responses of Fe−NO and N−O bond strengths to changes in environment and porphyrin structure appear to provide insight into the relationship between structure and {FeNO}^{6} reactivity in heme proteins.

Acknowledgment. We acknowledge access to the Computational Chemistry and Biology Network (CCBN) at NDSU, where the calculations were performed (NIH RR-16471). Financial support from USDA (ND05299, K.R.R.), Hermann Frasch Foundation (446-HF97, K.R.R.), NCRR (P20 RR15566, K.R.R.), and NIH (GM38401, W.R.S.) is also gratefully acknowledged. Finally, we wish to thank Professors Colin Andrew and Michael Page for their helpful discussions.

JA046942B